RSC Advances

PAPER

View Article Online
View Journal | View Issue

Cite this: *RSC Adv.*, 2020, **10**, 29061

Synthesis of magnetic core–shell Fe_3O_4@PDA@Cu-MOFs composites for enrichment of microcystin-LR by MALDI-TOF MS analysis†

Zhijian Li,[ab] Congcong Gong,[a] Panpan Huo,[a] Chunhui Deng *[c] and Shouzhi Pu*[a]

Microcystin-LR (MC-LR) is a toxin released from cyanobacteria in eutrophicated water. MC-LR is the most abundant and the most toxic among microcystins. In this work, core–shell structured copper-based magnetic metal–organic framework (Fe_3O_4@PDA@Cu-MOFs) composites were synthesized *via* a solvothermal reaction and a sol–gel method. The Fe_3O_4@PDA@Cu-MOFs composites showed ultra-high surface area, strong magnetic response and outstanding hydrophilicity. The Fe_3O_4@PDA@Cu-MOFs composites combined with matrix-assisted laser desorption/ionisation time-of-flight mass spectrometry (MALDI-TOF-MS) were used to analyse the content of MC-LR in real water samples. Under the optimised conditions, our proposed method exhibited good linearity within a concentration range of 0.05–4 μg L^{-1} and good detection even at low limits (0.015 μg L^{-1}). The method was also successfully applied to analyse traces of MC-LR with quantitative recoveries for the real water samples in the range from 98.67% to 106.15%. Furthermore, it was characterized by high sensitivity, short operation time, being environmental friendly and having the ability to analyse other pollutants in the environment.

Received 8th May 2020
Accepted 6th July 2020

DOI: 10.1039/d0ra04125d

rsc.li/rsc-advances

1 Introduction

In recent years, because of climate change and the increase of industrial and agricultural activities, environmental problems such as eutrophication of water bodies and cyanobacteria blooms have been causes for concern in water environments.[1–3] For example, since the 1980's, cyanobacterial blooms have frequently occurred in China, and they have affected the quality of drinking water used by people.[4–6] Additionally, they can produce several classes of toxins such as nodularin and microcystins.[7] Among the microcystins group, microcystin-LR (MC-LR) is one of the most toxic and commonly present toxins.[8,9] MC-LR can cause various diseases including skin allergies, acute gastroenteritis, diarrhoea, vomiting, pulmonary oedema and damage to the liver.[10] The World Health Organization (WHO) has assigned the tolerance limit concentration of 1 μg L^{-1} for MC-LR in drinking water.

To ensure water quality, several methods and techniques have been applied for MC-LR detection in water. Some of them are colorimetric aptamer assay,[11–13] high-performance liquid chromatography (HPLC),[14] enzyme-linked immunosorbent assay,[15,16] fluorescence biosensor immunoassay,[17,18] electrochemical.[19–21] Although these methods can detect exceedingly low levels of MC-LR, they always require harmful solvents and time-consuming, skilled and complex operating procedures. For example, HPLC is more precise than the other methods, but they require expensive equipment, operation complexity and long analysis time. Recently, matrix-assisted laser desorption/ionisation time-of-flight mass spectrometry (MALDI-TOF MS) has been widely applied for the detection and analysis of various compounds such as proteins,[22,23] peptides,[22,24] and small molecules[25,26] because it is a rapid, simple and sensitive technique. However, the detection limit of MALDI-TOF MS is high and this makes it unsuitable as per the WHO advisory level for drinking water.[27] Hence, a simple, rapid and efficient method for enriching MC-LR in drinking water by MALDI-TOF MS analysis is developed.

A variety of functionalised nanomaterials with high surface area and inner pores such as mesoporous carbon,[28] graphene[19] and mesoporous silica[29] have been applied to the enrichment of MC-LR in water samples and for environment analysis. In the meantime, metal–organic frameworks (MOFs) have been developed rapidly and attracted specific interests in separation of sample due to their outstand property. MOFs are a class of hybrid inorganic–organic porous crystalline materials formed by combining metal ions and organic ligands. They have attracted considerable attention because of their ultra-high surface areas, mesoporous structures, aromatic organic ligands and functional tenability. Thus, MOFs have been widely

[a]Jiangxi Key Laboratory of Organic Chemistry, Jiangxi Science and Technology Normal University, Nanchang 330013, PR China. E-mail: lizhijianhdd@163.com; pushouzhi@tsinghua.org.cn

[b]Shanghai Key Laboratory of Atmospheric Particle Pollution and Prevention, Department of Environmental Science and Engineering, Fudan University, Shanghai 200433, China

[c]Fudan University, Shanghai 200438, China. E-mail: chdeng@fudan.edu.cn

† Electronic supplementary information (ESI) available. See DOI: 10.1039/d0ra04125d

applied in various fields including gas storage and separation, drug delivery, catalysis, gas sensors, and adsorption and chromatographic techniques.[30,31]

Herein in this work, we designed and synthesized Fe_3O_4@PDA@Cu-MOFs by modifications step by step. Fe_3O_4 was employed to fast separation. Poly-dopamine (PDA) not only acted as the linker between Cu-MOFs and Fe_3O_4 but also increased the hydrophilicity. Cu-MOFs was constructed *via* coordination of copper ion and 1,3,5-benzenetricarboxylic acid. Cu-MOFs were linked to the surface of PDA by self-assembly. On the basis of boric Cu^{2+} specific affinity for carboxyl and amino groups, Fe_3O_4@PDA@Cu-MOFs was used as a substrate for enrichment of MC-LR and directly for MALDI-TOF MS analysis.

2 Experimental section

2.1. Chemicals and materials

Iron(III) chloride hexahydrate ($Fe_3Cl\cdot 6H_2O$), dopamine hydrochloride, 1,3,5-benzenetricarboxylic acid and *N*,*N*-dimethyformamide (DMF) were obtained from Sigma-Aldrich (St. Louis, MO, USA). Copper(II) acetate ($Cu(Ac)_2$), ethanol, sodium acetate (NaAc) and glycol were purchased from Sinopharm Chemical Reagent Co., Ltd (Shanghai, China). Microcystin-LR, tris(hydroxymethyl)aminomethane (Tris) and α-cyano-4-hydroxycinnamic acid (CHCA) were purchased from Sigma-Aldrich (St. Louis, MO, USA). Trifluoroacetic acid (TFA) and acetonitrile (ACN) were purchased from Merck (Darmstadt, Germany). Distilled water was purified by a Milli-Q system (Milford, MA, USA). Other chemicals were of analytical grade and were commercially available.

2.2. Synthesis of Fe_3O_4@PDA@Cu-MOFs microspheres

Fe_3O_4 microspheres were synthesised by a solvothermal reaction according to previous methods. Briefly, 0.675 g of $FeCl_3\cdot 6H_2O$ and 1.8 g of NaAc were dissolved in 75 mL of ethylene glycol and stirred for 30 min at room temperature to obtain a homogeneous mixture. Subsequently, the mixture was shifted to a 200 mL Teflon-lined stainless steel autoclave and hydrothermally treated at 200 °C for 16 h. After cooling to room temperature, the obtained magnetic particles were collected by a magnetic field and rinsed several times with deionised water and ethanol. The final products were dried in a vacuum.

Then, magnetic core–shell Fe_3O_4@PDA particles were synthesized accordingly to a previously reported procedure. First, 0.1 g of Fe_3O_4 particles was dispersed in a mixture containing 40 mL of H_2O and 40 mL of ethanol. The mixed solution was sonicated for 10 min. Subsequently, 0.05 g of Tris and 0.32 g of dopamine hydrochloride were added to the mixed solution, and the mixture was stirred for 16 h at room temperature. Then, the Fe_3O_4@PDA particles were collected using a magnet and rinsed several times with deionised water and ethanol. The obtained products were dried in vacuum at 50 °C for 12 h.

To prepare Fe_3O_4@PDA@Cu-MOFs, 0.075 g of Fe_3O_4@PDA particles were dispersed in 40 mL of DMF and sonicated for 10 min followed by an addition of 0.01 g of $Cu(Ac)_2\cdot H_2O$ and 0.12 g of 1,3,5-benzenetricarboxylic acid. The mixture was heated at 70 °C for 45 min. Finally, the Fe_3O_4@PDA@Cu-MOFs particles were collected by a magnet, washed thrice with ethanol and then dried in a vacuum for 12 h at 50 °C.

2.3. Characterisations and measurements

Transmission electron microscopy (TEM) was applied to characterise the morphology using a JEOL 2011 microscope (JEOL, Japan) at 200 kV. Scanning electronic microscopy (SEM) was performed using a Philips XL30 electron microscope (Netherlands) at 20 kV. Fourier transform infrared (FT-IR) spectra were collected on a Nicolet Fourier spectrophotometer (USA) using KBr pellets. Powder X-ray diffraction (XRD) was used to observe the composition and crystallisation of Fe_3O_4@PDA@Cu-MOFs using a Bruker D4 X-ray diffractometer with Ni-filtered Cu Kα radiation (40 kV, 40 mA) (Germany). Nitrogen adsorption–desorption isotherms were performed on a Micromeritics Tristar 3000 analyser (USA) at 77 K. The Brunauer–Emmett–Teller (BET) method was applied to calculate the specific surface area of the sample. X-ray photoelectron spectra (XPS) were collected on an RBD 147 upgraded PHI 5000C ESCA system with a dual X-ray source (Shimadzu Corp). A Mg Kα (1253.6 eV) anode and a hemispherical energy analyser were used in the measurement. All the binding energies were referenced to the 1s peak at 284.8 eV of the surface adventitious carbon.

2.4. Enrichment of MC-LR using Fe_3O_4@PDA@Cu-MOFs

A series of MC-LR standard solutions (0.01, 0.05, 0.1, 0.5, 1, 2, 4, 8 and 16 μg L^{-1}) were prepared and 1 mg of Fe_3O_4@PDA@Cu-MOFs composite was added to 1 mL of ultra-pure water to obtain a 1 mg mL^{-1} solution of Fe_3O_4@PDA@Cu-MOFs composites. Then, 20 μL of the 1 mg mL^{-1} Fe_3O_4@PDA@Cu-MOFs solution and 80 μL of different concentrations MC-LR solutions was mixed and vibrated for 30 min. Subsequently, the Fe_3O_4@PDA@Cu-MOFs composites enriched with MC-LR were collected by a magnet. The Fe_3O_4@PDA@Cu-MOFs composites were washed by elution.

2.5. MALDI-TOF MS analysis

All the MALDI-TOF MS experiments were recorded on a 5800 MALDI-TOF MS (Applied Biosystems, Framingham, MA, USA) equipped with a Nd:YAG laser (383 nm) in positive reflector mode. The instrument was operated at an acceleration voltage of 20 kV. The parameters of MALDI-TOF MS were set as follows: laser intensity, 60%; mass range, 700–1500 *m*/*z*. A ground-steel sample target with 384 spots was utilised, and 1 μL of the eluate was deposited on the MALDI plate and dried at room temperature. After that, 1 μL of the CHCA solution was deposited onto the layer of the eluate and dried. The MALDI plate was analysed by MALDI-TOF MS.

2.6. Analysis of MC-LR real water sample

To further confirm their superior enrichment efficiency for MC-LR, Fe_3O_4@PDA@Cu-MOFs microspheres were applied to real water sample. The real water samples were obtained from the Poyang Lake in China. The real water sample was centrifuged

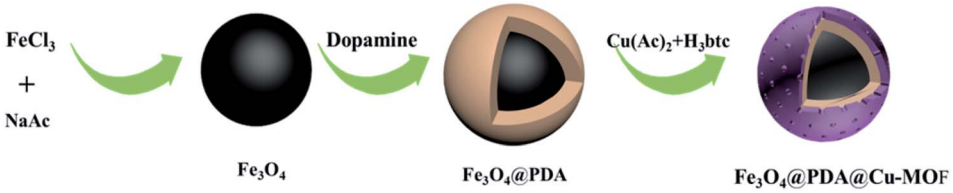

Scheme 1 The synthetic route of the Fe_3O_4@PDA@Cu-MOFs microspheres.

for 5 min at 10 000 rpm to remove large particles. 20 μL of the 1 mg mL^{-1} Fe_3O_4@PDA@Cu-MOFs composite was added 80 μL real water sample mixed and vibrated for 30 min, after the enriched MC-LR were separated by magnet, followed by washing with deionized water (50 μL) three times to remove other compounds. The obtained Fe_3O_4@PDA@Cu-MOFs-MC-LR was eluted with 10 μL for 10 min. Finally, the eluted MC-LR was directly transferred onto plate for MALDI-TOF MS analysis.

3 Results and discussion

Scheme 1 describes the synthesis route of the Fe_3O_4@PDA@Cu-MOFs microspheres. First, strongly magnetic Fe_3O_4 nanoparticles were synthesised through a hydrothermal reaction. Then, the PDA layer was decorated onto the surface of Fe_3O_4 because it contains hydroxyl and amino groups that can combine with metal ions. Subsequently, the Cu-MOFs were modified onto the surface of Fe_3O_4@PDA by using sol–gel method. Because PDA has good hydrophilicity and excellent dispersibility, it not only improved the hydrophilicity but also acted as the linker between Cu-MOFs and Fe_3O_4. Finally, the Fe_3O_4@PDA@Cu-MOFs composites were used as adsorbent for the enrichment of MC-LR in water samples on the basis of the reaction of Cu^{2+} with carboxyl and amino groups.

The morphologies and size of Fe_3O_4, Fe_3O_4@PDA and Fe_3O_4@PDA@Cu-MOFs were characterised by SEM and TEM. As shown in Fig. 1a, the TEM image of Fe_3O_4 revealed that the average particle size of Fe_3O_4 was approximately 100 nm. The Fe_3O_4@PDA microspheres showed a typical core–shell structure with a PDA shell of approximately 15 nm (Fig. 1b). The TEM images of Fe_3O_4@PDA@Cu-MOFs in Fig. 1c show that Cu-MOFs are coated on the surface of Fe_3O_4@PDA. The TEM images of Fe_3O_4@PDA@Cu-MOFs indicate that the thickness of the Cu-MOFs shell is approximately 20 nm. Moreover, the SEM observation shows that Fe_3O_4@PDA@Cu-MOFs have spherical morphology (Fig. S1†).

Fig. S2† shows the FT-IR spectra of Fe_3O_4, Fe_3O_4@PDA and Fe_3O_4@PDA@Cu-MOFs. In all the samples, the peaks at 3398 cm^{-1} and 557 cm^{-1} were assigned to the O–H stretching vibration of hydroxyl groups and Fe–O–Fe stretching vibration of Fe_3O_4.[32] For Fe_3O_4@PDA, the bands at 1385 cm^{-1} and 1588 cm^{-1} were attributed to the C–N stretching vibration and C=C vibration of the aromatic ring indicating the successful formation of PDA on the surface of Fe_3O_4 (Fig. S2b†). Besides, relative to the Fe_3O_4@PDA composites, the FT-IR spectra of Fe_3O_4@PDA@Cu-MOFs show other adsorption bands at 1400 cm^{-1} and 3418 cm^{-1}, which could be because to the O–H stretching vibration and O–H bending vibration of carboxyl groups from Cu-MOFs.

The XRD pattern of Fe_3O_4@PDA@Cu-MOFs is shown in Fig. 2. The peaks at $2\theta = 30.4°$, 35.6°, 43.3°, 53.7°, 57.3° and 62.7° can be indexed to the (220), (311), (400), (422), (511) and (440) reflections of the cubic Fe_3O_4 phase, respectively, (JCPDS card no. 190629).[33] Moreover, the peaks at $2\theta = 10.7°$, 12.6°, 13.9°, 19.9°, 25.1° and 27.3° can be indexed to the (222), (331), (422), (731), (751) and (440) planes of Cu-MOFs, respectively.[34]

XPS was used to examine the compositions of the surface elements and electronic state of Fe_3O_4@PDA@Cu-MOFs. As shown in Fig. 3a, O, Cu and C could be observed, but no peaks that corresponded to Fe appeared, thereby, proving that the magnetic Fe_3O_4 core was well encapsulated inside the core–shell microspheres by PDA@Cu-MOFs. The C 1s spectrum of Fe_3O_4@PDA@Cu-MOFs (Fig. 3c) exhibited peaks at 284.6 eV,

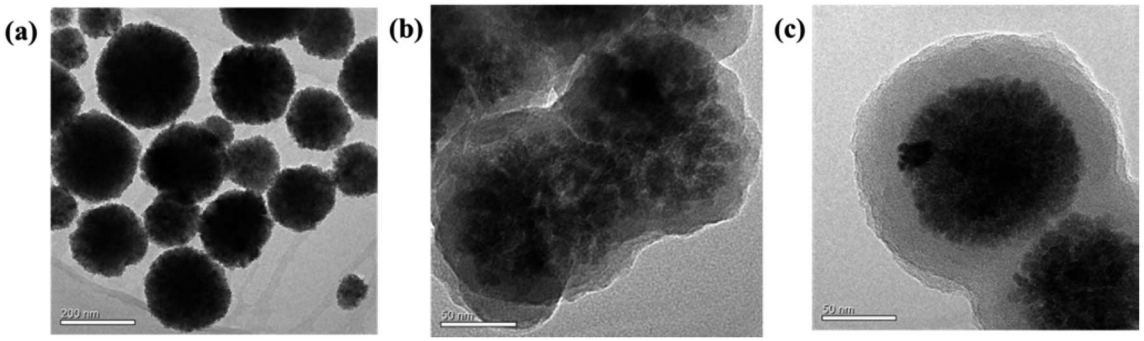

Fig. 1 TEM images of (a) Fe_3O_4, (b) Fe_3O_4@PDA and (c) Fe_3O_4@PDA@Cu-MOFs.

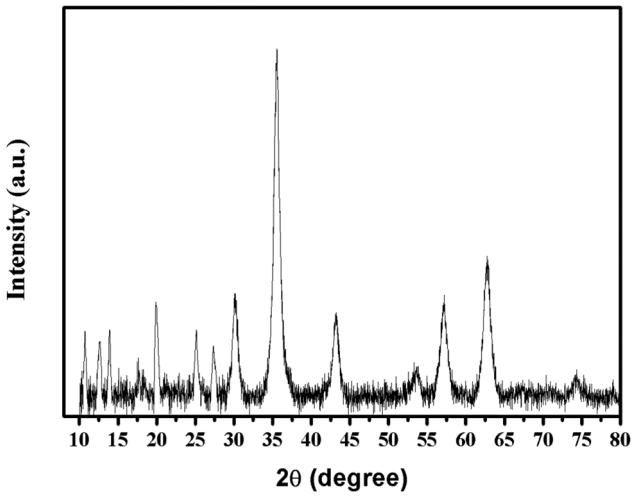

Fig. 2 XRD pattern of Fe_3O_4@PDA@Cu-MOFs.

287.3 eV and 289.2 eV, which can be attributed to C=C, C=O and O–C=O, respectively. The XPS peaks of Cu 2p that centred at 933.7 eV and 953.6 eV (Fig. 3b) can be assigned to Cu $2p_{3/2}$ and Cu $2p_{1/2}$, respectively. In addition, two characteristic peaks centred at 943.4 eV and 938.8 eV, which could be attributed to the satellite peaks of Cu 2p.[35] The peaks of O 1s at 529.7 eV and 531.5 eV could be ascribed to the lattice oxygen (C–O) and O–H of Cu-MOFs, respectively (Fig. 3d). The mass percentages of C, O, N and Cu were determined to be 66.75%, 24.50%, 4.54% and 4.21%, respectively. These results indicate that Cu-MOFs were successful decorated onto the surface of Fe_3O_4@PDA.

The inner architectures of the Fe_3O_4@PDA@Cu-MOFs composites were investigated by nitrogen adsorption–desorption isotherm analysis. As exhibited in Fig. 4a, Fe_3O_4@PDA@Cu-MOFs gave rise to a type-IV curve, which indicated that the Fe_3O_4@PDA@Cu-MOFs composites had a mesoporous structure. The Brunauer–Emmett–Teller (BET) surface area and total pore volume of the Fe_3O_4@PDA@Cu-MOFs composites were calculated to be 70.4 $m^2\ g^{-1}$ and 0.055 $cm^3\ g^{-1}$, respectively. The pore size distributions derived from the adsorption branches of the isotherms by using the Barrett–Joyner–Halenda (BJH) model displayed a mean pore size of approximately 3.2 nm (Fig. 4b). Taken together, these results indicate that the Fe_3O_4@PDA@Cu-MOFs composites had large surface area and a mesoporous structure.

Eluents have a considerable effect on desorption from the Fe_3O_4@PDA@Cu-MOFs adsorbent. Three common eluents were used to investigate the effect of elution of MC-LR (*i.e.* 50% CAN-0.1% TFA (v : v), 0.25 M NH_4HCO_3 and 0.4 M $NH_3 \cdot H_2O$). Fig. 5 shows that the effect of elution of MC-LR desorbed by 0.25 M NH_4HCO_3 were higher than 50% CAN-0.1% TFA and 0.4 M $NH_3 \cdot H_2O$ under the same condition. These results suggest that 0.25 M NH_4HCO_3 is the optimising eluent for desorption of MC-LR from the enriched by Fe_3O_4@PDA@Cu-

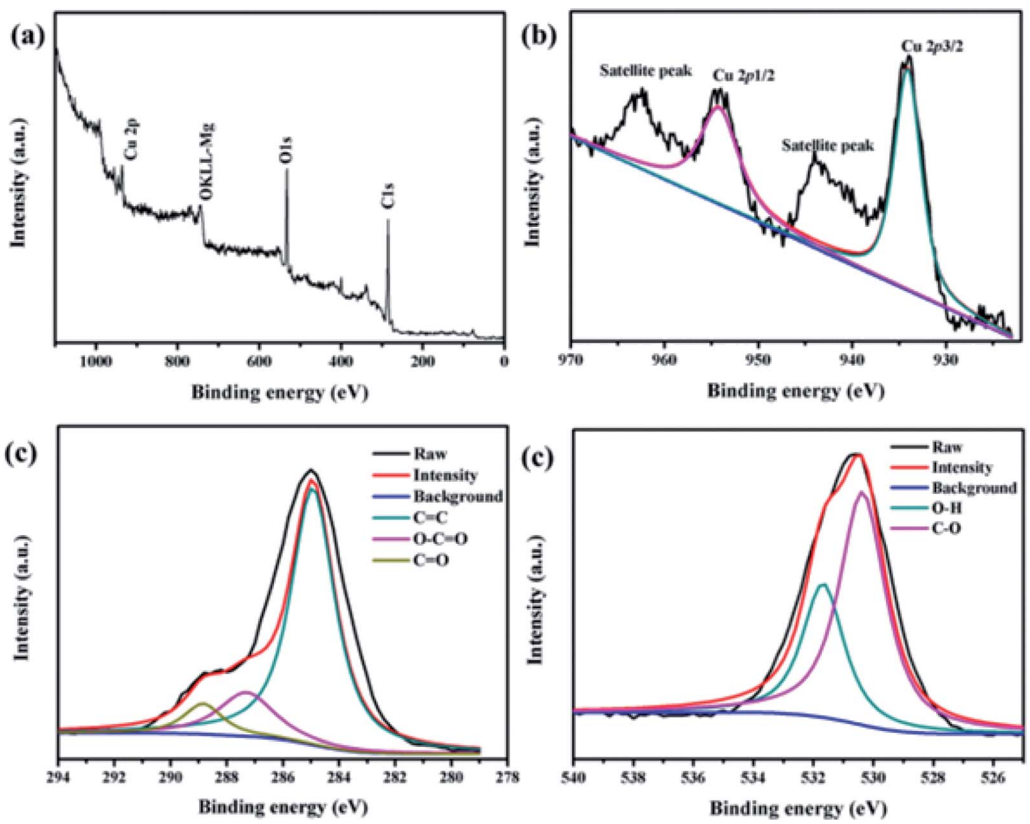

Fig. 3 XPS spectra of the Fe_3O_4@PDA@Cu-MOFs composites: (a) wide XPS survey spectrum, (b) Cu 2p, (c) C 1s and (d) O 1s.

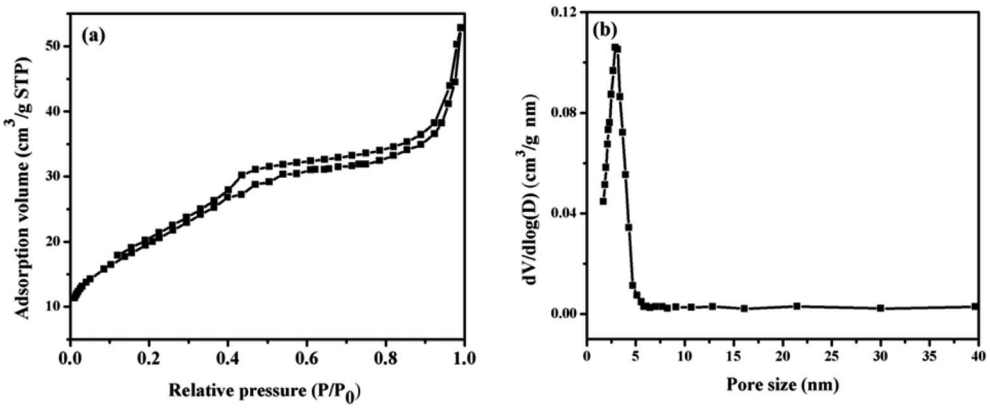

Fig. 4 Nitrogen adsorption–desorption isotherms (a) and pore size distributions of the Fe_3O_4@PDA@Cu-MOFs composites (b).

MOFs composites. Therefore, ammonium bicarbonate eluents were used in the following experiments.

The enrichment procedure for MC-LR by using the Fe_3O_4@PDA@Cu-MOFs composites is shown in Scheme 2. The MALDI-TOF MS signal intensity of 1 μg L^{-1} MC-LR is shown in Fig. S3a,† the signal intensity is 365. After enrichment by the Fe_3O_4@PDA@Cu-MOFs composites, the signal intensity is 3754 (Fig. S3b†), the results indicate that an enrichment factor of about 10. Under the optimised eluent condition, the Fe_3O_4@PDA@Cu-MOFs composites for enrichment and detection MC-LR were studied. As shown in Fig. 6a, the mass signal intensities increased with the increase MC-LR concentration. The result showed that the signal intensity of MC-LR had good linearity ($R^2 = 0.997$) with the logarithm of MC-LR concentration from 0.05 μg L^{-1} to 4 μg L^{-1}. The linear regression equation was determined to be $Y = 2279.07 + 1344.52 \log C_{\text{MC-LR}}$ (μg L^{-1}). The limit of detection (LOD) was 0.015 μg L^{-1} (LOD = $3\sigma/k$, k is the slope of the calibration curve and σ is the standard

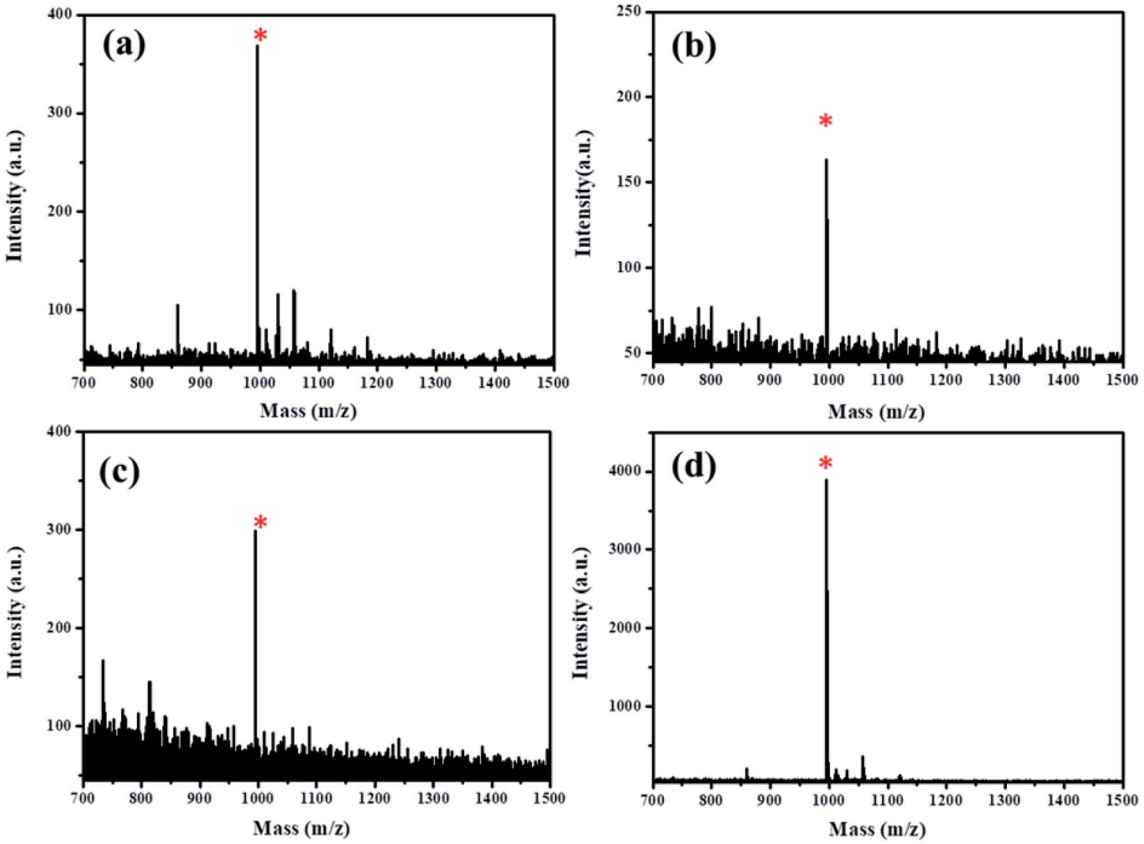

Fig. 5 MALDI-TOF MS of the 1 μg L^{-1} MC-LR solution treated with the Fe_3O_4@PDA@Cu-MOFs composites with different eluents: deionized water (a); 50% CAN-0.1% TFA (v : v) (b); 0.25 M NH_4HCO_3 (c); 0.4 M $NH_3 \cdot H_2O$ (d). (* represents the signal of MC-LR.)

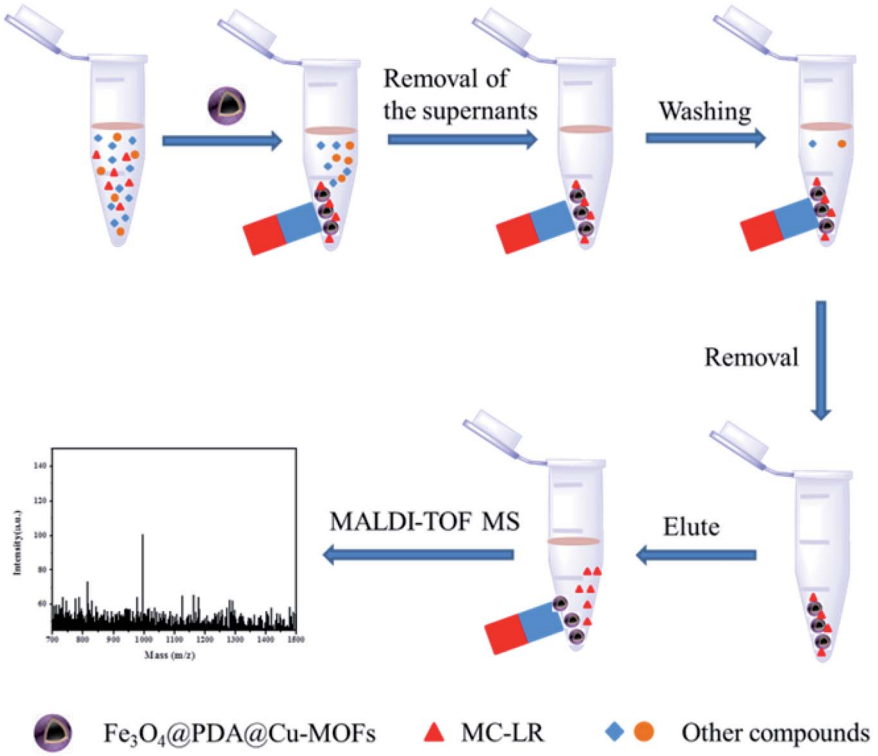

Scheme 2 Enrichment process of MC-LR by MALDI-TOF MS analysis.

deviation), which was lower than the maximum limit of MC-LR in drinking water specified by WHO. As depicted in Table S1,† our method afforded better results than others methods, which were previously reported.

To evaluate the applicability of the present method in real water samples, the MC-LR content in real water samples was determined by MALDI-TOF MS before and after enrichment using the Fe_3O_4@PDA@Cu-MOFs composites (Fig. S4†). MC-LR was not detected in the mass spectrum of the water sample before treatment with the Fe_3O_4@PDA@Cu-MOFs composites (Fig. S4a†). In contrast, MC-LR was detected after treatment with the Fe_3O_4@PDA@Cu-MOFs composites (Fig. S4b†), which indicated that the Fe_3O_4@PDA@Cu-MOFs composites could successfully enrich the MC-LR content in real water samples. According to the established calibration equations, the recoveries were 98.68–106.2% for MC-LR (Table 1). These results demonstrate that the Fe_3O_4@PDA@Cu-MOFs composites have great potential to be used for the analysis of MC-LR in real water samples by MALDI-TOF MS spectroscopy.

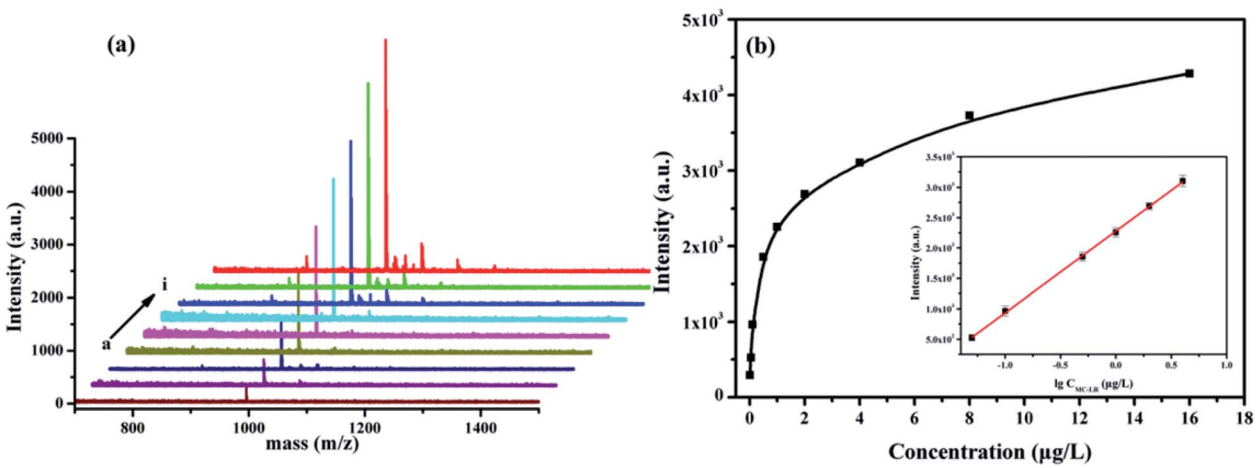

Fig. 6 MALDI-TOF MS response signal intensities plotted with different concentrations of MC-LR ((a–i) 0.01, 0.05, 0.1, 0.5, 1, 2, 4, 8 and 16 μg L^{-1}) (a) and the corresponding calibration plots (b). The inset of (b) is corresponding linear relationship from 0.05 to 4 μg L^{-1}.

Table 1 Recovery and corresponding relative standard deviation (RSD) of the MC-LR

Analyte	Added (μg L^{-1})	Found (μg L^{-1})	Recovery (%)	RSD (n)
MC-LRs	1	1.062	106.2	6.1
	2	2.010	100.5	8.2
	4	3.947	98.68	6.6

4 Conclusions

In summary, Fe_3O_4@PDA@Cu-MOFs composites were successfully synthesised *via* a solvothermal reaction and a sol–gel method. The Fe_3O_4@PDA@Cu-MOFs composites exhibited excellent hydrophilicity, high surface area, strong magnetism and a mesoporous structure. They were applied as adsorbents for the enrichment of low-concentration MC-LR in real water samples and directly for MALDI-TOF MS analysis. This method earned good linear range, low detection limit and intermediate precision for MC-LR, indicating that the Fe_3O_4@PDA@Cu-MOFs composites can used as suitable sorbents for MC-LR in water. All the above results indicated that Fe_3O_4@PDA@Cu-MOFs composites as adsorbent have great promise in environmental field.

Conflicts of interest

There are no conflicts to declare.

Acknowledgements

This work was financially supported by the Science and Technology Research Project of Education Department of Jiangxi Province and the Natural Science Foundation of Jiangxi Province (20171ACB20025, GJJ190615). We was also grateful for the Shanghai Key Laboratory of Atmospheric Particle Pollution and Prevention (FDLAP19004).

Notes and references

1 N. L. McLellan and R. A. Manderville, *Toxicol. Res.*, 2017, **6**, 391–405.
2 Z. Svirčev, D. Drobac, N. Tokodi, B. Mijović, G. A. Codd and J. Meriluoto, *Arch. Toxicol.*, 2017, **91**, 621–650.
3 X. Yan, X. Xu, M. Wang, G. Wang, S. Wu, Z. Li, H. Sun, A. Shi and Y. Yang, *Water Res.*, 2017, **125**, 449–457.
4 B. Qin, G. Zhu, G. Gao, Y. Zhang, W. Li, H. W. Paerl and W. W. Carmichael, *Environ. Manag.*, 2010, **45**, 105–112.
5 G. A. Codd and P. B. Nunn, *Toxicon*, 2019, **168**, 93–94.
6 Y. Zhou, J. Yuan, J. Wu and X. Han, *Toxicol. Lett.*, 2012, **212**, 48–56.
7 J. Ma, Y. Li, H. Duan, R. Sivakumar and X. Li, *Chemosphere*, 2018, **192**, 305–317.
8 R. Yang, D. Song, S. Fang, Y. Liu, X. Zhou, F. Long and A. Zhu, *Biosens. Bioelectron.*, 2018, **121**, 27–33.
9 S. Karthikeyan, D. D. Dionysiou, A. F. Lee, S. Suvitha, P. Maharaja, K. Wilson and G. Sekaran, *Catal. Sci. Technol.*, 2016, **6**, 530–544.
10 M. J. Brophy, A. L. Mackie, Y. Park and G. A. Gagnon, *Environ. Sci.: Processes Impacts*, 2019, **21**, 659–666.
11 X. Li, R. Cheng, H. Shi, B. Tang, H. Xiao and G. Zhao, *J. Hazard. Mater.*, 2016, **304**, 474–480.
12 A. Sassolas, G. Catanante, D. Fournier and J. L. Marty, *Talanta*, 2011, **85**, 2498–2503.
13 A. C. Neumann, X. Wang, R. Niessner and D. Knopp, *Anal. Methods*, 2016, **8**, 57–63.
14 L. Spoof, K. Karlsson and J. Meriluoto, *J. Chromatogr. A*, 2001, **909**, 225–236.
15 J. Zhang, J. Lei, R. Pan, C. Leng, Z. Hu and H. Ju, *Chem. Commun.*, 2011, **47**, 668–670.
16 Z.-L. Xu, S.-L. Ye, L. Luo, X. Hua, J.-X. Lai, X.-P. Cai, Q.-W. Liang, H.-T. Lei, Y.-M. Sun, Y.-p. Chen and X. Shen, *Sci. Total Environ.*, 2020, **708**, 134614.
17 Y. Zhang, Y. Lai, X. Teng, S. Pu, Z. Yang, P. Pang, H. Wang, C. Yang, W. Yang and C. J. Barrow, *Anal. Methods*, 2020, **12**, 1752–1758.
18 Y. Zhang, Z. Zhu, X. Teng, Y. Lai, S. Pu, P. Pang, H. Wang, C. Yang, C. J. Barrow and W. Yang, *Talanta*, 2019, **202**, 279–284.
19 L. Tang, X. Ouyang, B. Peng, G. Zeng, Y. Zhu, J. Yu, C. Feng, S. Fang, X. Zhu and J. Tan, *Nanoscale*, 2019, **11**, 12198–12209.
20 K. Abnous, N. M. Danesh, M. A. Nameghi, M. Ramezani, M. Alibolandi, P. Lavaee and S. M. Taghdisi, *Biosens. Bioelectron.*, 2019, **144**, 111674.
21 T. Guan, W. Huang, N. Xu, Z. Xu, L. Jiang, M. Li, X. Wei, Y. Liu, X. Shen, X. Li, C. Yi and H. Lei, *Sens. Actuators, B*, 2019, **294**, 132–140.
22 M. Zhao, C. Deng and X. Zhang, *ACS Appl. Mater. Interfaces*, 2013, **5**, 13104–13112.
23 A. Maus, R. Mignon and F. Basile, *Anal. Biochem.*, 2018, **545**, 31–37.
24 L. Ling, C. Xiao, S. Wang, L. Guo and X. Guo, *Talanta*, 2019, **200**, 236–241.
25 Z. Li, Q. Liu, X. Lu, C. Deng, N. Sun and X. Yang, *Talanta*, 2019, **194**, 329–335.
26 H. Zhao, Y. Li, J. Wang, M. Cheng, Z. Zhao, H. Zhang, C. Wang, J. Wang, Y. Qiao and J. Wang, *ACS Appl. Mater. Interfaces*, 2018, **10**, 37732–37742.
27 S. Liu, C. Deng and X. Zhang, *Talanta*, 2016, **154**, 183–189.
28 W. Teng, Z. Wu, J. Fan, H. Chen, D. Feng, Y. Lv, J. Wang, A. M. Asiri and D. Zhao, *Energy Environ. Sci.*, 2013, **6**, 2765–2776.
29 W. Teng, Z. Wu, D. Feng, J. Fan, J. Wang, H. Wei, M. Song and D. Zhao, *Environ. Sci. Technol.*, 2013, **47**, 8633–8641.
30 C. Hu, M. He, B. Chen, C. Zhong and B. Hu, *J. Chromatogr. A*, 2013, **1310**, 21–30.
31 A. Amiri, R. Tayebee, A. Abdar and F. Narenji Sani, *J. Chromatogr. A*, 2019, **1597**, 39–45.
32 Y. Deng, C. Deng, D. Qi, C. Liu, J. Liu, X. Zhang and D. Zhao, *Adv. Mater.*, 2009, **21**, 1377–1382.
33 X. Lou and L. Archer, *Adv. Mater.*, 2008, **20**, 1853–1858.
34 M. Zhao, X. Zhang and C. Deng, *Chem. Commun.*, 2015, **51**, 8116–8119.
35 Z. Wang, M. Gui, M. Asif, Y. Yu, S. Dong, H. Wang, W. Wang, F. Wang, F. Xiao and H. Liu, *Nanoscale*, 2018, **10**, 6629–6638.